

Reaction route control by microperoxidase-9/CTAB micelle ratios†

Tatiana Prieto,^a Rodrigo O. Marcon,^a Fernanda M. Prado,^b Antonio C. F. Caires,^a
Paolo Di Mascio,^b Sergio Brochsztain,^a Otaciro R. Nascimento^c and
Iseli L. Nantes^{*a}

Received 3rd February 2006, Accepted 28th February 2006

First published as an Advance Article on the web 14th March 2006

DOI: 10.1039/b601671e

Microperoxidases (MP) as water-soluble models attract interest to studying the reaction mechanism of peroxidases because these heme peptides are able to form the same enzyme intermediates during the reaction with peroxides. In this work we have demonstrated that the association of Fe(III)MP-9 and Fe(III)MP-11 with CTAB micelles (MP-9/CTAB and MP11/CTAB) provides a microenvironment with an alkaline interface and a hydrophobic core that exhibits peroxidase behavior. This microenvironment shifts positively the redox potential of microperoxidases by ~ 100 mV. *tert*-Butylhydroperoxide (*t*-BuOOH) when added to the medium, converted Fe(III)MP-9/CTAB to MP-9/CTAB Compound II, a high valence oxidized intermediate of the heme peptide. Subsequent addition of diphenylacetaldehyde (DPAA) to MP-9/CTAB Compound II regenerated the native form of the enzyme, Fe(III)MP-9/CTAB, what characterizes the occurrence of a peroxidase cycle. Fe(III)MP-9/CTAB regenerated during the peroxidase cycle reacted with residual DPAA in the medium to form Fe(II)MP-9/CTAB, which indicates that both Fe(III)MP-9/CTAB and its oxyferryl form can use aldehydes as reducing agents. According to the determined reduction potential, Fe(III)MP-9 and Fe(III)MP-9/CTAB should be able to oxidize DPAA (reduction potential -630 mV). The reaction of MP-9/CTAB with DPAA produced benzophenone as final product, detected by infrared spectroscopy and mass spectrometry. Interestingly, a significant difference was observed in the benzophenone yield according to the micelle/MP-9 molar ratio.

Introduction

Peroxidases are enzymes that contain the heme group as catalytic center and use peroxides as oxidizing agents to generate their reactive high-valency intermediates. There are two superfamilies of peroxidases: the first one encompasses plant, fungal and (archae) bacterial peroxidases and the second one encompasses the mammalian peroxidases whose secondary and tertiary structures as well as the prosthetic group differ significantly from those of plant or fungal peroxidases.¹ A unique characteristic of the mammalian peroxidases is the presence of covalent bonds between the heme group and the protein. In myeloperoxidase, lactoperoxidase, eosinophil peroxidase, and probably thyroid peroxidase these covalent links are two ester bonds between aspartic or glutamic amino acid residues and hydroxyl groups on the 1- and 5-methyl groups of the heme.^{2,3} Myeloperoxidase has also a third covalent bond between one of its vinyl groups and the

methionine residue. It has been demonstrated that the covalent bonds can be formed by an autocatalytic process involving reaction of the apoprotein–heme complex with substrates.^{2,3} Peroxidases also differ by the nature of the proximal heme iron ligand.^{1–5} These structural characteristics influence the catalytic properties of the peroxidases.^{1,4,5}

Interesting models of peroxidases can be obtained by sequential pepsin- and trypsin-catalyzed hydrolysis of horse-heart cytochrome *c* and they are known as microperoxidases. The product of the hydrolysis retains the heme group covalently attached to cysteine residues 14 and 17.^{6–8} Four microperoxidase types were identified according to the sequence of native cytochrome *c*, from which these peptide fragments are derived: microperoxidase-6, (CAQCHT), -8, (CAQCHTVE), -9 (KCAQCHTVE) and -11 (VQKCAQCHTVE). Microperoxidases exist in the ferric resting states, retain histidine as a fifth heme iron ligand but not the methionine residue at the sixth coordination position which, in this case, at neutral pH, is occupied by a water molecule. The absence of methionine 80 at the sixth coordination position of microperoxidases favors the peroxidase activity of the hemepeptide.^{6–8} Scheme 1, below, shows the structure of microperoxidase-9.

Because these structural characteristics, microperoxidases have been useful to study structural and catalytic properties of peroxidases and cytochromes^{9,10} as well as to develop electrode sensors.¹¹

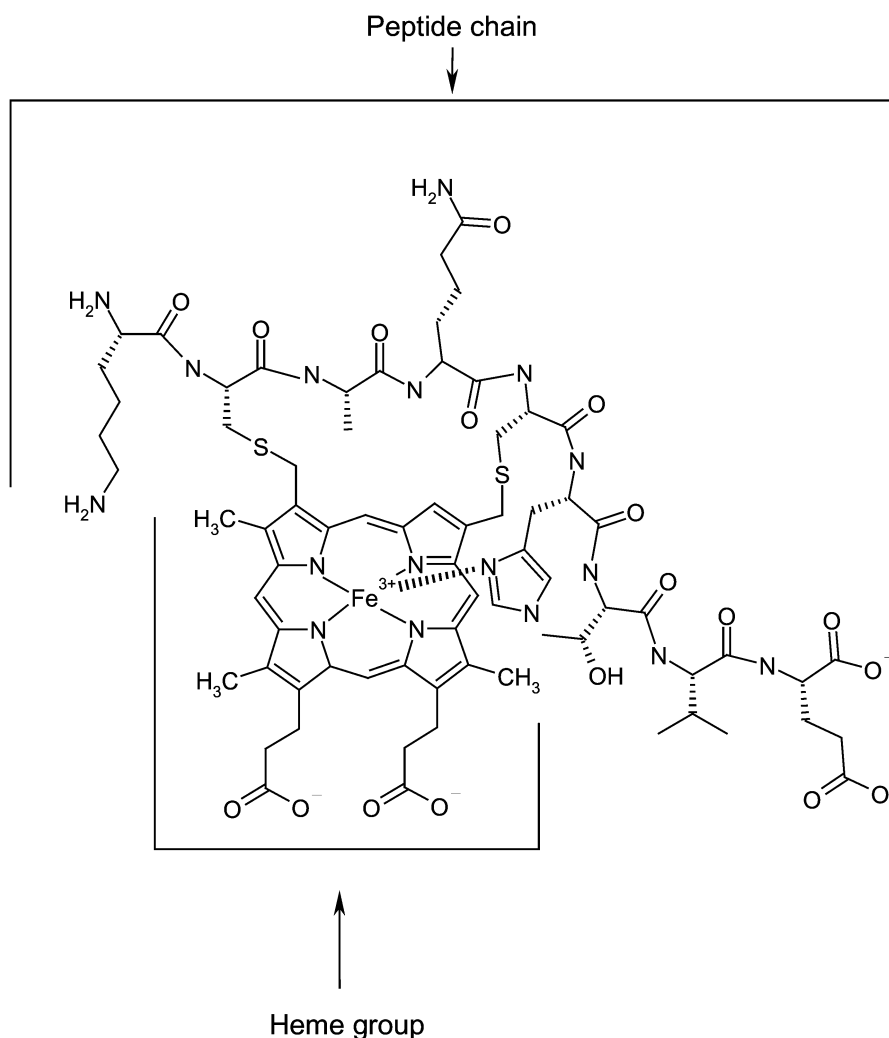
Similarly to biological peroxidases, microperoxidase-8 is able to convert a wide variety of organic compounds at the

^a Centro Interdisciplinar de Investigação Bioquímica-CIIB Universidade de Mogi das Cruzes-UMC, Mogi das Cruzes – SP, Brazil. E-mail: ilnantes@umc.br; Fax: +55-11-4798-7068; Tel: +55-11-4798-7102

^b Depto de Bioquímica, Instituto de Química, Universidade de São Paulo, USP-São Paulo – SP, Brazil

^c Grupo de Biofísica, Instituto de Física de São Carlos, Universidade de São Paulo, USP-São Carlos, São Carlos – SP, Brazil

† Electronic supplementary information (ESI) available: Electrochemical data of microperoxidases in phosphate buffer and CTAB micelles (Tables S1–S4; Fig. S1). See DOI: 10.1039/b601671e



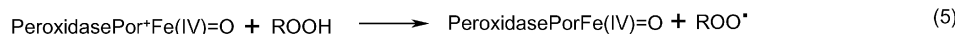
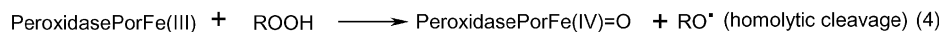
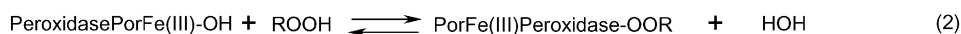
Scheme 1 The structure of MP-9.

expense of hydrogen peroxide (H_2O_2) in a type of peroxidase chemistry.¹² Similarly to horseradish peroxidase (HRP), microperoxidases can react with peroxides and produce the intermediate compounds 0, I and II of HRP.^{13,14} Compound 0 has been detected for HRP at low temperature and corresponds to the porphyrin iron-hydroperoxide (Por-Fe(III)-OOR) species.¹³ This species precedes the formation of Compounds I (Por⁺Fe(IV)=O) and II (PorFe(IV)=O) which are well-known high-valent intermediates of peroxidases.^{14,15} Compound II can react with a reducing agent leading to the regeneration of the native peroxidase form. This reaction pathway is known as peroxidase cycle. The first step of the peroxide cleavage promoted by peroxidases is the formation of Compound 0 in which the deprotonated water at the sixth coordination position was replaced by the hydroperoxide [Scheme 2, eqn (1) and (2)]. After the formation of Compound 0, there are two possible mechanisms for the cleavage of peroxides (ROOH): a heterolytic cleavage generating the alcohol derivative (ROH) and Compound I (Scheme 2, eqn (3)), which reacts with another peroxide molecule generating Compound II and the peroxy radical (ROO[•]) (Scheme 2, eqn (5)) or a homolytic cleavage of ROOH to

form Compound II directly (Scheme 2, eqn (4)). Whatever the mechanism for peroxide cleavage, native Fe(III)peroxidase can be regenerated after the reaction of Compound II with another ROOH molecule or another reducing agent (Scheme 2, eqn (6)).^{13–15}

It is known that protons in the distal heme active site influence the formation of the catalytic reactive species for both peroxidases and cytochrome P450.¹⁶ In HRP, the distal His42 ligand acts as an acid/base catalyst that favors the deprotonation of the hydroperoxide substrate at the enzyme active site (Compound 0) and the subsequent heterolytic cleavage.^{17–19} Therefore, the deprotonation of the hydroperoxide in Compound 0 is a crucial step in the catalytic cycle of peroxidases and cytochrome P450.

A competitive effect of protons has been demonstrated for the reaction of Fe(III) or Mn(III)MP-8 with hydrogen peroxide, suggesting that Compound 0 precedes the formation of a high-valent intermediate of Fe(III) or Mn(III)MP-8.²⁰ In comparison with HRP, MP-8 in aqueous medium does not exhibit a site pocket with a distal basic residue participating in the peroxide deprotonation and favoring the O–O peroxide bond cleavage. These characteristics could somehow be responsible for the



Scheme 2 Proposed mechanism for the benzophenone production from DPAA oxidation by MP-9/CTAB.

low reactivity of MP-8 at low pH. In aqueous medium, alkaline pH leads to deprotonation of the MP-8 bound water, which then either assists concerted hydrogen peroxide deprotonation and coordination of the hydroperoxo group to the metal center or is directly oxidized by hydrogen peroxide to a metal-hydroperoxo MP-8.²⁰

Recently we have demonstrated that the association of microperoxidases-8 and -9 to CTAB micelles provides a protein-like hydrophobic environment to the heme group, which allows this complex to exhibit the catalytic properties of the peroxidases.^{21,22} The association of Fe(III)MP-8 with CTAB micelles provides a microenvironment with an alkaline interface and a hydrophobic core that gives special characteristics to the Fe(III)MP-8/peroxide (*tert*-butylhydroperoxide (*t*-BuOOH) or H₂O₂) reaction as compared to homogeneous medium. The reaction of Fe(III)MP-8 with *t*-BuOOH and H₂O₂ produced alkoxy and hydroxyl radicals as the initial radicals, respectively. These free radicals are produced presumably by homolytic scission of the O–O bond by Fe(III)MP-8/CTAB. The UV-visible spectral changes detected for Fe(III)MP-8 during the reaction with peroxides point to the formation of Compound II as the species that exhibits subsequent bleaching. The K_m and the maximal conversion rate (k_2) of CTAB-bound Fe(III)MP-8 into the corresponding Compound II were determined for the reaction with peroxides in 20 mM CTAB, at pH 7.4 and 9.1. For both substrates, the K_m values increased at pH 9.1 without significant changes in k_2 values, indicating alteration on the affinity of the substrates for CTAB-bound Fe(III)MP-8.²¹ In another work we reproduced the HRP catalytic cycle for MP-9 associated to CTAB micelles. The addition of *t*-BuOOH to the medium containing MP-9 associated to CTAB micelles led to the occurrence of a peroxidase cycle, indicating that this aggregate behaves as a true enzyme.²² In this work, for the first time, we present the reduction potential of MP-9 in CTAB micelles followed by a study of the one electron oxidation of diphenylacetaldehyde by MP-9 associated to CTAB micelles.

Materials and methods

Chemicals

Microperoxidase-9, *t*-BuOOH and CTAB were obtained from Sigma Chemical Co. (St Louis, MO, USA). All aqueous

solutions were prepared with deionized water (mixed bed of ion exchanger, Millipore) and the pH was measured using a combined glass electrode (Orion Glass pH SURE-FLOW™). The reference electrode (ROSS™, model 8102) was filled with Orion Filling Solution (ROSS™). The pH meter was calibrated using METREPAK pHydriion standard buffer solutions (Brooklyn, NY).

Preparation of micellar CTAB solutions

CTAB micellar solutions were prepared by dissolving CTAB in an appropriate buffer with stirring at 37 °C. The CMC (critical micelle concentration) was determined in the usual fashion from plots of the surface tension *vs.* log [CTAB]. Surface tensions were measured with DeNoüy tensiometer equipped with a Pt ring.

Cyclic voltammetry measurements

Cyclic voltammetry was performed by using AUTOLAB PGSTAT30 potentiostat. All measurements were carried out at room temperature (25 ± 2 °C) in a three-compartment electrochemical cell consisting of a glass carbon disk (0.07 cm² area) as a working electrode, a platinum auxiliary electrode and a Ag/AgCl reference electrode in 3 M KCl solutions. Argon bubbling was used to remove oxygen from the solutions in the electrochemical cell. The diffusion coefficient (D_0) was calculated from the slope of the curve obtained from the plot of i_{pc} (A) *vs.* the square root of the sweep rate (mV) according the Randles–Sevcik equation (eqn (1))

$$i_{pc} = (2.687 \times 10^5) n^{3/2} \nu^{1/2} D^{1/2} AC$$

where 2.687×10^5 is a constant when the temperature is 298.15 K ($\text{C mol}^{-1} \text{V}^{-1/2}$), n = number of electrons appearing in half-reaction for the redox couple, ν is the rate at which the potential is swept (V s^{-1}), A = the electrode area (cm²) and C (mol cm^{-3}) is the concentration of the redox species.

UV-visible measurements

Solutions of Fe(III)MP-9 and the corresponding H₂O₂ or *t*-BuOOH solutions were both buffered with 5 mM sodium phosphate. The concentration of Fe(III)MP-9 was verified by using $\epsilon_{397} = 1.57 \times 10^5 \text{ M}^{-1} \text{ cm}^{-1}$ for Fe(III)MP-8 at pH 7.0.²³ The concentration of Fe(III)MP-9 in CTAB micelles was calculated by using $\epsilon_{400} = 1.13 \times 10^5 \text{ M}^{-1} \text{ cm}^{-1}$, determined

from a standard curve obtained by registering the spectra of Fe(III)MP-8/CTAB at different hemepeptide concentrations.²²

Time-resolved spectra were recorded on a Shimadzu Model 1501 MultiSpec (Tokyo, Jp), employing the photodiode array scan mode. The spectral resolution was 0.5 nm and the spectra were obtained with a time interval of 1 s. According to microperoxidase concentration, the optical path length was 0.1 or 1 cm. The data sets represent the average of three independent measurements. The kinetic data were recorded at 417 nm for Fe(III)MP-9/CTAB, the region of strong absorbance of the Compound II species.

Heme iron EPR measurements

Direct EPR measurements of Fe(III)MP-9 (100 μ M) were obtained in a Bruker ELEXSYS EPR system E-580 under the following conditions: gain 5×10^3 , modulation amplitude 1.0 mT, microwave power 4 mW, temperature 11 K, time constant 20.48 ms and conversion time 81.92 ms. After mixing, solutions were quickly introduced into an EPR quartz tube that was previously cooled in liquid nitrogen. After freezing the sample was introduced into the microwave cavity at low temperature and the EPR measurements were performed.

Fourier transform infrared (FTIR) spectrometry

The spectra of the samples were recorded on a Perkin-Elmer spectrometer mod. Spectrum One. The benzophenone spectra were obtained by using KBr pellets technique in the region of 4000–400 cm^{-1} with a resolution of 4 cm^{-1} . The spectra of MP Schiff bases were measured by using ATR technique, in the region of 4000–650 cm^{-1} with a resolution of 2 cm^{-1} . A monocrystal of ZnSe, 45°, was utilized as optical element of internal reflexion.

Mass spectrometry analysis of benzophenone

Benzophenone was analyzed by a Quatro II Micromass mass spectrometer with Z-spray™ ion source (Manchester, UK). The analysis of benzophenone was done by using acetonitrile–formic acid 0.1% (1 : 1, v/v) by electrospray ionization (ESI) in the positive ion mode. The source and desolvation temperatures were 120 and 150 °C, respectively. The parameters of the equipment were: sample cone voltage at 30 V, extraction cone voltage at 5 V and capillary potential at 3.5 kV. Full scan data were acquired over a mass range of 100–300 m/z . The data were processed by the Mass Lynx NT data system, Version 3.2 (Micromass, Manchester, UK).

Results

Fig. 1 shows the cyclic voltammograms of 100 μ M MP-9 and MP-11 in the absence and in the presence of CTAB (dashed, dotted, thin solid and thick solid lines, respectively). The presence of CTAB micelles shifted the MP-11 $E_{1/2}$ from –346 to –276 mV. Similar results were obtained with MP-9. MP-9 exhibited $E_{1/2} = -346$ mV in the absence of CTAB and this value changed to –231 mV in the presence of CTAB (Fig. 1).

In the presence of CTAB micelles, the minimal ΔE_p was ~ 57 mV obtained at 10 mV s^{-1} suggesting a fully reversible one-electron-transfer reaction. The inset of Fig. 1 shows that

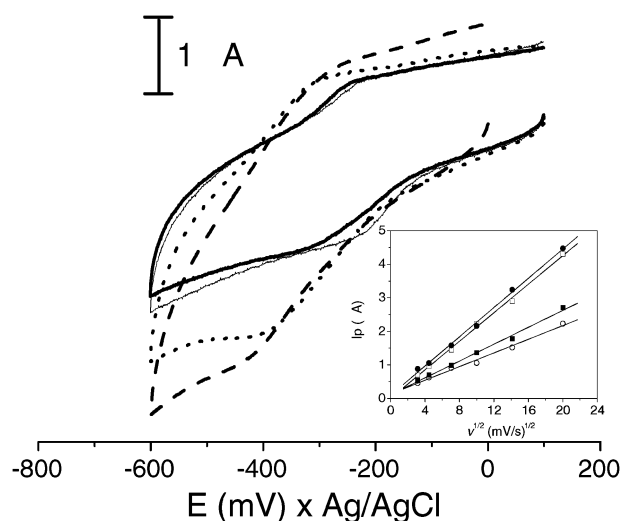


Fig. 1 Cyclic voltammetry of MP-9 and MP-11 in the absence and in the presence of CTAB (dashed line: MP-9 in phosphate buffer, dotted line: MP-9 in CTAB micelles, thin solid line: MP-11 in phosphate buffer and thick solid line: MP-11 in CTAB micelles). The peptides were present at a concentration of 0.1635 mg mL^{-1} . Phosphate buffer (0.02 M) at pH 7.4 was present in all samples. In the absence of CTAB 25 μ M of MgCl_2 was added to the samples. The data were acquired over the potential range of 100 to –600 mV vs. Ag/AgCl, with sweep rate of 50 mV s^{-1} and temperature of 25 °C. The electrode area was 0.07 cm^2 . The inset shows a plot of i_p vs. (scan rate).²

in the presence and in the absence of CTAB, both MP-11 and MP-9 exhibit i_{pc} proportional to the square root of the scan rate and thus the redox process of microperoxidases at the electrode surface could be considered diffusion-controlled. From the slope of the curves, the values of D_o for both MP-11 and MP-9 diffusion coefficient were calculated. In the absence of CTAB, D_o was the same for both microperoxidases ($1.5 \times 10^{-5} \text{ cm}^2 \text{ s}^{-1}$), and in the presence of CTAB, D_o values obtained were 3.7×10^{-6} and $5.6 \times 10^{-6} \text{ cm}^2 \text{ s}^{-1}$ for MP-9 and MP-11, respectively.

The redox potential exhibited by MP-11 and MP-9 in homogeneous and heterogeneous media suggests that these hemepeptides in the native form (Fe(III)) and in the high valence forms, *i.e.*, Compound I and Compound II, should be able to oxidize aldehydes such as diphenylacetaldehyde (DPAA) with $E_{1/2} = -630$ mV (cyclic voltammogram not shown).

The addition of *t*-BuOOH to a medium containing Fe(III)MP-9 associated to CTAB micelles (Fig. 2A, thin solid line) led to the conversion of the native form of the hemepeptide to its high valence intermediate Compound II (oxoferryl form, thick solid line in Fig. 2A). According to previous work,²² in this experimental condition, MP-9 Compound II returned to the native form but the regeneration of the native form was accompanied by discrete bleaching of the Soret band (Fig. 2A, dashed line), probably due to the attack of free radicals produced in the course of the reaction. However, when 10 or 600 μ M diphenylacetaldehyde (DPAA) was added to the medium after the accumulation of MP-9/CTAB Compound II (Fig. 2B and C, thick solid lines), the regeneration of Fe(III)MP-9/CTAB (Fig. 2B and C, dotted lines) was faster

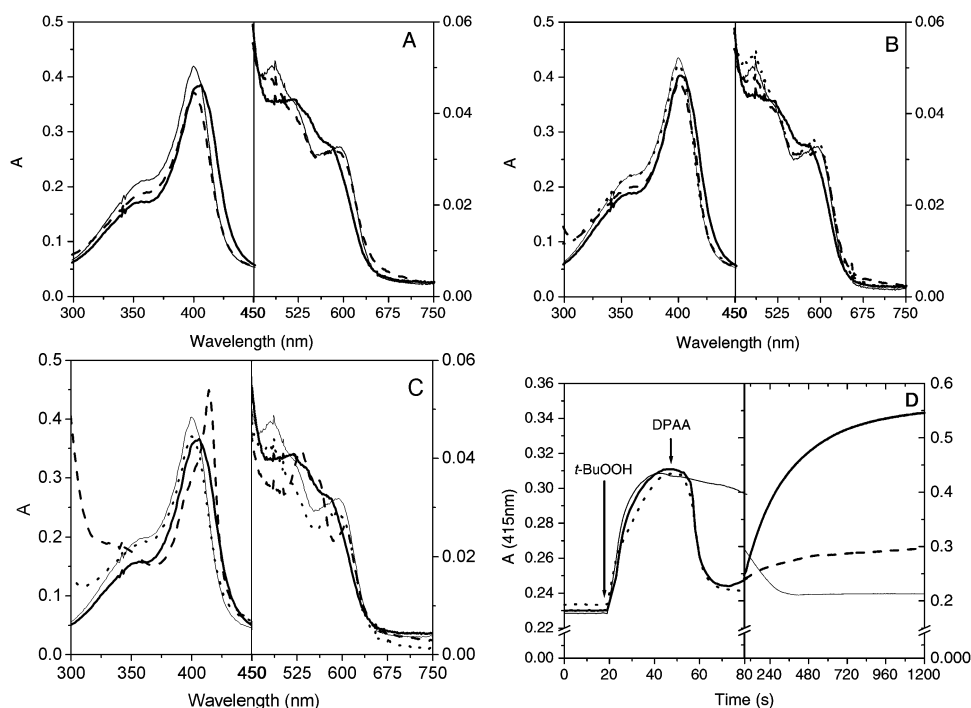


Fig. 2 (A) MP-9 spectral changes during the peroxidase cycle. Thin solid line: Fe(III)MP-9 associated to CTAB micelles. Thick solid line: MP-9 Compound II associated to CTAB micelles, 20 s after addition of 10 μM *t*-BuOOH. Dashed line: Fe(III)MP-9 associated to CTAB micelles recovered 3.5 min after addition of 10 μM *t*-BuOOH. (B) MP-9 spectral changes during the peroxidase cycle. Thin solid line: Fe(III)MP-9 associated to CTAB micelles. Thick solid line: MP-9 Compound II associated to CTAB micelles, 20 s after addition of 10 μM *t*-BuOOH. Dashed line: Fe(III)MP-9 associated to CTAB micelles recovered 50 s after addition of 10 μM DPAA. Dotted line: Fe(III) and Fe(II)MP-9 associated to CTAB micelles obtained 20 min after the addition of 10 μM DPAA. (C) MP-9 spectral changes during the peroxidase cycle. Thin solid line: Fe(III)MP-9 associated to CTAB micelles. Thick solid line: MP-9 Compound II associated to CTAB micelles, 20 s after addition of 10 μM *t*-BuOOH. Dashed line: Fe(III)MP-9 associated to CTAB micelles recovered 50 s after addition of 600 μM DPAA. Dotted line: Fe(II)MP-9 associated to CTAB micelles obtained 20 min after the addition of 600 μM DPAA. The experiments were carried out with 20 mM CTAB, 2.5 μM MP-9, in 5 mM phosphate buffer, pH 7.4 at 25 $^{\circ}\text{C}$ by using a 1 cm optical path length cuvette. (D) Kinetic profiles of MP-9/CTAB catalytic cycle obtained in the conditions described in (A) (thin solid line), (B) (dashed line) and (C) (thick solid line).

(rate = $2.7 \times 10^{-3} \Delta A_{415\text{nm}} \text{ s}^{-1}$) than in the absence of DPAA (rate = $0.4 \times 10^{-3} \Delta A_{415\text{nm}} \text{ s}^{-1}$). Thus, the comparison of the regeneration rate in the presence and in the absence of the aldehyde revealed that DPAA accelerated the enzyme catalytic cycle. Fe(III)MP-9 recovered at the cycle end, when the *t*-BuOOH should be depleted, reacted with residual DPAA in a concentration dependent manner to form Fe(II)MP-9/

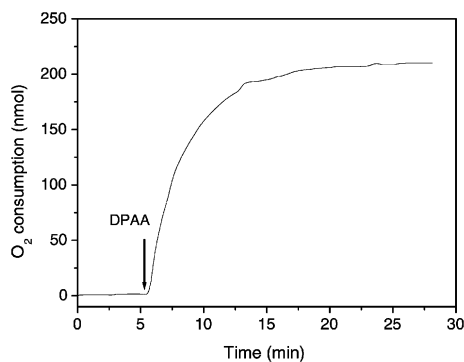
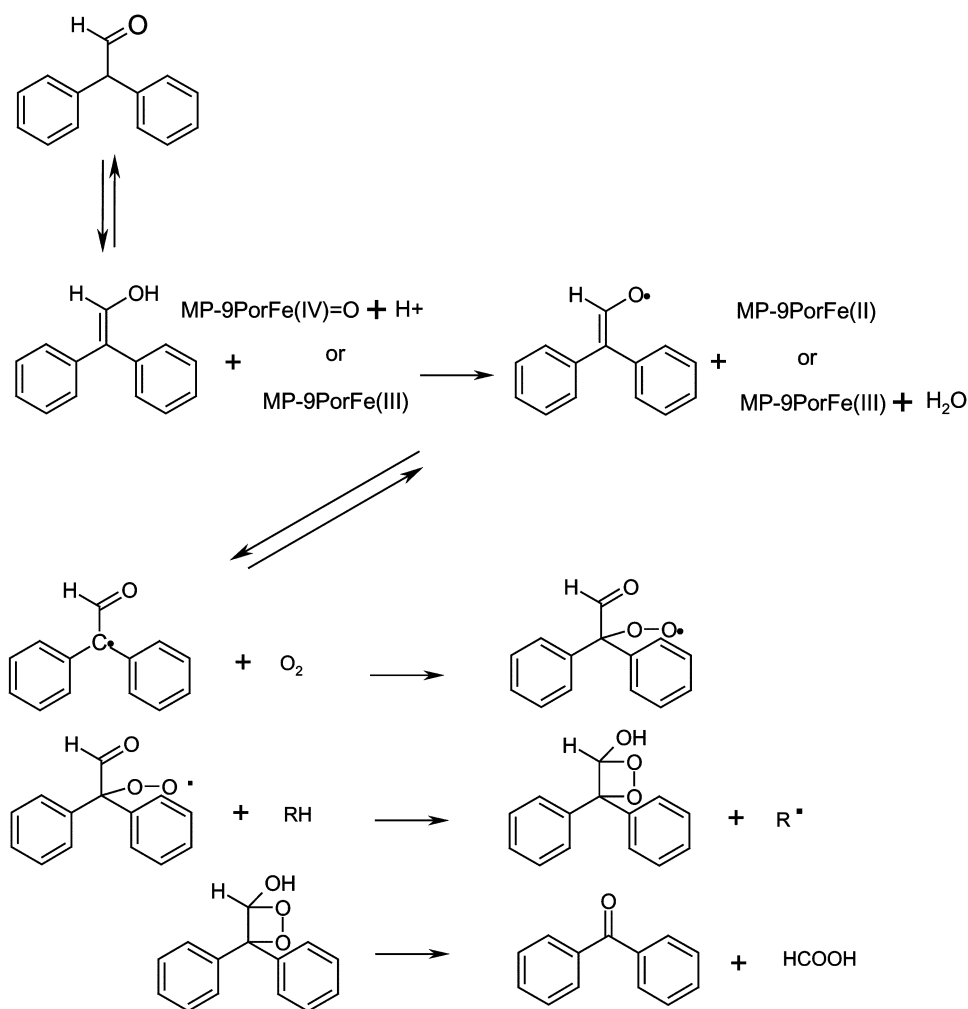


Fig. 3 Oxygen consumption during the reaction of MP-9/CTAB with DPAA. The experiment was carried out at 25 $^{\circ}\text{C}$, in 5 mM phosphate buffer, pH 7.4, with 2.5 μM MP-9, 20 mM CTAB and 600 μM DPAA added to the medium at the time indicated by the arrow.

CTAB (Fig. 2C, dashed line). The kinetic profiles of the MP-9 catalytic cycle in the absence and in the presence of 10 and 600 μM diphenylacetaldehyde are shown in Fig. 2D, thin solid, dashed and thick solid lines, respectively. Similar results were obtained in different MP-9 and CTAB micelle concentrations (not shown). The reaction of MP-9/CTAB with *t*-BuOOH and DPAA, in a micelle/peptide ratio of 6.0, was also accompanied by continuous-wave EPR of heme iron. Similarly to previous reports,^{21,22} the heme iron EPR spectra obtained after *t*-BuOOH addition exhibited decrease of the signal compatible with the formation of compound II, an EPR silent species. In the absence of DPAA, the signal of the Fe(III) heme iron was recovered, coherent with the occurrence of the peroxidase catalytic cycle.²² However, in the presence of DPAA the EPR signal was lost again concomitantly with the formation of Fe(II)MP-9/CTAB, also an EPR silent species (not shown).

Considering that oxygen consumption was detected during the reaction of DPAA with MP-9/CTAB (Fig. 3), we propose a reaction mechanism in which benzophenone is the final reaction product (Scheme 3).

However, the reaction of DPAA with the amino groups present in the MP-9 structure to form Schiff base adducts could not be overlooked. In this regard, interesting differences were observed by comparing the reaction carried out in the



Scheme 3 Oxidation of diphenylacetaldehyde by Compound II MP-9/CTAB and native MP-9/CTAB.

presence of micelle/MP-9 molar ratio ~ 66.0 with the reaction in the presence of micelle/MP-9 molar ratio ~ 6.0 . In the presence of the micelle/MP-9 molar ratio ~ 66.0 , the addition of DPAA led to a fast increase in the absorbance at 254 nm (thin solid line in Fig. 4A), accompanied by a concomitant increase in the fluorescence of the sample (inset). In the presence of the micelle/MP-9 molar ratio ~ 6.0 , the addition of DPAA led to the enhancement of the absorbance at 260 nm (thin solid line) with a kinetic profile similar to that observed for the heme iron reduction (thick solid line in Fig. 4B). Fig. 4C shows the spectral differences observed for the MP-9/CTAB complexes in different micelle/hemepeptide ratios. Fig. 4C shows that the decrease of the micelle/hemepeptide ratio led to the red shift of Soret and Q bands, suggesting the formation of aggregates with at least one pair of MP-9 per micelle. Fig. 4D shows the corresponding EPR spectra of MP-9/CTAB in the micelle/MP-9 ratios 0.5 and 5.0. The parameters obtained from the EPR spectra (see Discussion) corroborate that different MP-9/CTAB high spin states are favored in different micelle/MP-9 ratios. The results described above suggest that benzophenone production was predominant in the presence of micelle/MP-9 molar ratio ~ 6.0 , whereas Schiff base adduct was predominant in the presence

of micelle/MP-9 molar ratio ~ 66.0 . In fact, during the reaction of MP-9 CTAB with DPAA, when the micelle/MP-9 molar ratio was ~ 6.0 , it was evident the precipitation of crystals at the bottom of the tube (Photo as Fig. 1 of Supplemental Materials). The production of benzophenone as the final product was corroborated by infrared spectroscopy (Fig. 5) and mass spectrometry analysis (Fig. 6) of the material that precipitated during the reaction. Fig. 5 shows the IR spectra of pure benzophenone (solid line) and the spectrum of the material that precipitated and in which benzophenone and residual DPAA were probable present. The vibrational spectrum of pure benzophenone shows a strong absorption band (4.3% T) at 1652 cm^{-1} , due to the normal vibrational mode of the functional group $-\text{C}=\text{O}$ stretching. The aromatic ring conjugation changes the absorption of this group to a lower frequency comparatively to aliphatic ketones. Bending appears as a sharp band at 1323 cm^{-1} (12.7% T). Absorption due to vibrational normal modes of $=\text{C}-\text{H}$ stretching for sp^2 C-H out-of-plane can be observed in the $3087\text{--}3055\text{ cm}^{-1}$ region. A pair of ring stretch absorption is noted at 1593 and 1573 cm^{-1} . The IR spectrum of the product precipitated during the reaction and containing a mixture of benzophenone and DPAA exhibits a strong absorption band (51.5% T)

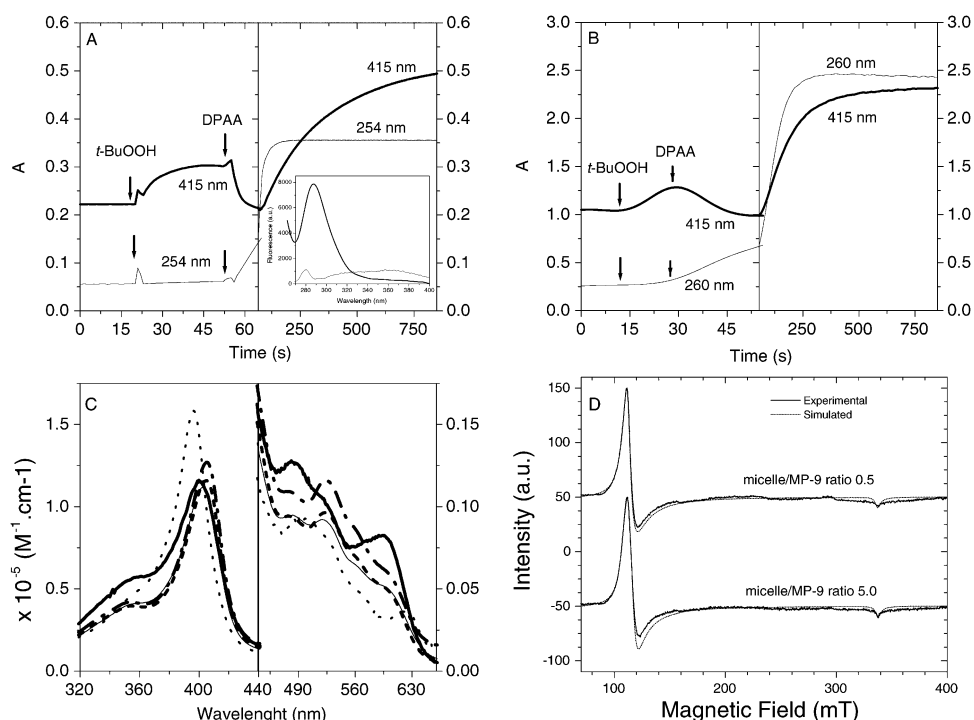


Fig. 4 (A) Kinetic profile of the MP-9/CTAB heme iron reduction concomitant with the formation of Schiff base adduct obtained with MP-9/CTAB molar ratio ~ 66.0 by using $20 \mu\text{M}$ *t*-BuOOH and 0.6 mM DPAA. Thick solid line corresponds to alterations in the Soret band intensity at 415 nm due to changes in the heme iron redox state. The thin solid line corresponds to alterations in the absorbance intensity at 254 nm due to the formation of Schiff base adducts. (B) Kinetic profile of the MP-9/CTAB heme iron reduction concomitant with the formation of Schiff base adduct obtained with MP-9/CTAB molar ratio ~ 6.0 by using $300 \mu\text{M}$ *t*-BuOOH and 20 mM DPAA. The thick solid line corresponds to alterations in the Soret band intensity at 415 nm due to changes in the heme iron redox state. Thin solid line corresponds to alterations in the absorbance intensity at 260 nm due to the formation of benzophenone. The addition of the peroxide and the aldehyde is indicated by the arrows. (C) Effect of the micelles/hemepeptide ratio on the MP-9 Soret and Q bands. Dotted line: Fe(III)MP-9 absence of CTAB at pH 7.4 The spectrum was obtained with $2.5 \mu\text{M}$ MP-9 and presented in ϵ units. Thick solid line: Fe(III)MP-9/CTAB when the CTAB/hemepeptide ratio was 50.0 . The spectrum was obtained with $2.5 \mu\text{M}$ MP-9 and presented in ϵ units. Thin solid line: Fe(III)MP-9/CTAB when the CTAB/hemepeptide ratio was 5.0 . The spectrum was obtained with $100 \mu\text{M}$ MP-9 and presented in ϵ units. Dashed line: Fe(III)MP-9/CTAB when the CTAB/hemepeptide ratio was 0.5 . The spectrum was obtained with $100 \mu\text{M}$ MP-9 and presented in ϵ units. Dashed-dotted line: Fe(III)MP-9/CTAB when the CTAB/hemepeptide ratio was 0.25 . The spectrum was obtained with $100 \mu\text{M}$ MP-9 and presented in ϵ units. (D) Direct EPR measurements of Fe(III)MP-9 ($100 \mu\text{M}$) in the presence of CTAB and in the micelle/MP-9 ratio = 0.5 and 5.0 . The spectra were obtained in a Bruker ELEXSYS EPR system E-580 under the following conditions: gain 5×10^3 , modulation amplitude 1.0 mT , microwave power 4 mW , temperature 11 K , time constant 20.48 ms and conversion time 81.92 ms . For the ratio of 0.5 , the frequency was 9.47445 GHz , g -values were 6.019 , 5.949 and 2.009 with 320.0 , 750.0 and $80.0/g(\text{D})\text{H}$ (MHz) and the line was adjusted with a Lorentzian shape. For the ratio of 5.0 , the frequency was 9.47298 GHz , the g -values 6.079 , 5.820 and 2.006 with 450.0 , 440.0 and $80.0/g(\text{D})\text{H}$ (MHz) and the lines were adjusted with Lorentzian shape.

relative to functional carbonyl group of the aldehyde at 1724 cm^{-1} and a stretch of aldehyde hydrogen ($-\text{CHO}$) at 2849 cm^{-1} (41.0% T). However the presence of the high intensity band (56.0% T) at 1658 cm^{-1} ($\nu-\text{C}=\text{O}$ of aromatic ketones), as well as the absorption band at 2849 cm^{-1} (41.0% T) can be assigned to the presence of high concentration of benzophenone mixed with residual DPAA.

Fig. 6 shows the mass spectrum of the material that precipitated during the reaction of MP-9/CTAB (micelles/MP-9 ratio = 6.0) with DPAA. The material was recorded in the positive ion mode with a cone voltage of 30 V exhibiting a peak with m/z 183 which corresponds to the pseudomolecular ion of benzophenone ($[\text{M} + \text{H}]^+ = 183$) and the peak with m/z 167 that represents the loss of the oxygen atom ($[(\text{M}-\text{O}) + \text{H}]^+ = 167$). The formation of MP-9 Schiff base adducts during the reaction with DPAA when the micelle/hemepeptide ratio was 66.0 was also corroborated by mass

spectrometry recorded in the positive ion mode with a cone voltage of 10 V exhibiting signals corresponding to MP-9 molecular ion, $[\text{M} + \text{H}]^+ = 1635$ and the corresponding adduct with DPAA molecular ion, $[\text{M} + \text{H}]^+ = 1834$ (spectra not shown). The IR analysis of MP-9 after the reaction with DPAA, in conditions in which the formation of Schiff base adducts was favored (Fig. 7), revealed a strong band at 1634 cm^{-1} attributed to the vibrational normal mode of the $-\text{C}=\text{N}-$ group of the Schiff bases.²⁴ Aromatic Schiff bases absorb in IR region near 1630 cm^{-1} ²⁵ and generally, the $\text{C}=\text{N}$ bands exhibit signal with intensity similar to that observed for $\text{C}=\text{O}$ and $\text{C}=\text{C}$ bands. The vibrational spectrum of DPAA-modified MP-9 revealed also an intense absorption band at 857 cm^{-1} , characteristic of angular deformation of the $\text{C}-\text{H}$ groups in the phenyl rings. Another intense band, attributed to the $\text{C}=\text{C}$ stretching of the phenyl rings, was detected at 1538 cm^{-1} . The results described above

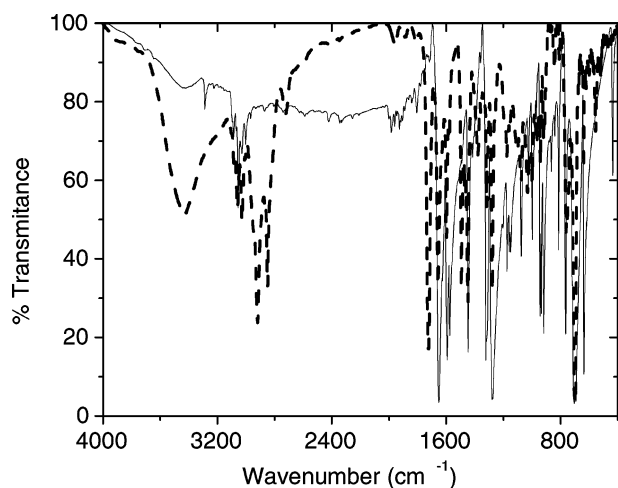


Fig. 5 Comparative FTIR spectra of benzophenone and the product of the reaction between MP-9/CTAB (hemepeptide/micelle ratio = 6.0) and DPAA. The dashed line represents the spectrum of the product that precipitated at the end of the reaction between MP-9/CTAB and DPAA. The solid line represents the spectrum of pure benzophenone.

corroborated the formation of DPAA-promoted Schiff bases in the MP-9 structure when the micelle/hemepeptide ratio was 66.0.

Discussion

The association of microperoxidases with CTAB micelles improves the catalytic activity of the enzyme.

The occurrence of peroxidase catalytic cycle during the reaction of MP-9/CTAB with *t*-BuOOH shows that this aggregate hemepeptide/micelle²² behaves as an artificial enzyme that we have named lipoenzyme. The catalytic cycle observed when peroxide (in this case, *t*-BuOOH) was the only substrate available implicates that the peroxide acts as the oxidizing

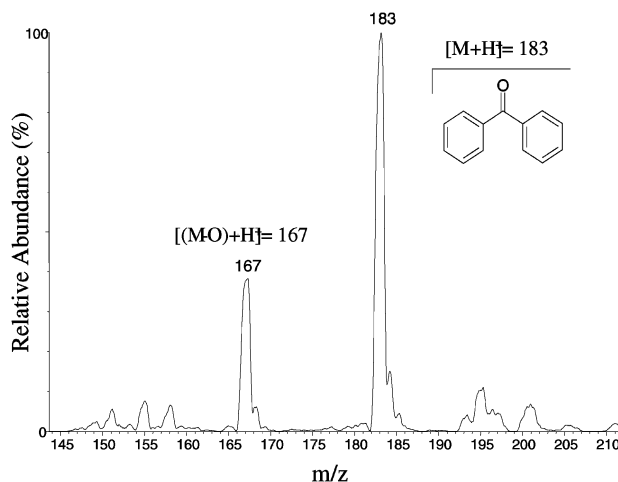


Fig. 6 ESI mass spectrum of the product obtained after the reaction between MP-9/CTAB (hemepeptide/micelle ratio = 6.0) and DPAA. The analysis was recorded in the positive ion mode with sample cone voltage and extraction cone voltage at 30 and 5 V, respectively.

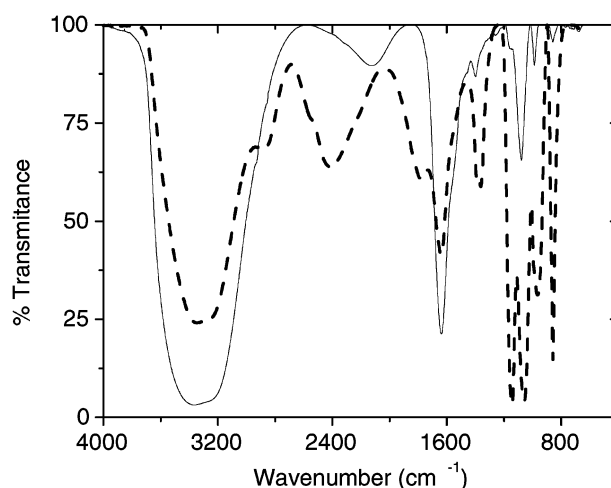


Fig. 7 Comparative FTIR spectra of MP-9 (solid line) and MP-9 with Schiff base obtained after the reaction with DPAA when hemepeptide/micelle ratio = 66.0 (dashed line).

(formation of Compound I) and the reducing agent (formation of Compound II and regeneration of the native form) of the prosthetic group, a phenomenon previously observed for peroxidases. Therefore, associated to CTAB micelles, microperoxidases behave as true peroxidases. In this regard, the hydrophobic core provided by CTAB micelles changed the redox potential of the microperoxidases to more positive values and made the lipoenzyme a better oxidizing agent as compared with microperoxidases in homogeneous medium (Fig. 1). The decrease of the catalytic efficiency (k_{cat}/K_M) previously observed for the cleavage of peroxides was due to the partition of these compounds inside and outside the micelles. In the case of DPAA, the highly hydrophobic compound, the partition occurs preferentially inside the micelles and the redox potential of the enzyme was the limiting factor of the catalytic efficiency.

Literature data have shown that, differently from metalloproteins that need the presence of appropriate promoters such as 4,4'-bipyridyl to achieve best electron transfer at the electrode,²⁶ microperoxidases exhibit rapid, reversible electron transfer at the electrode in the absence of mediators or promoters. This behavior has been attributed to the simpler and disordered conformation of microperoxidases, in which the heme group is exposed to the solvent. In the case of MP-11 it was previously reported that the hemepeptide takes part in a rapid one-electron reaction at the glassy carbon electrode in the absence of mediators. In this condition, the smallest ΔE_p value obtained was about 90 mV indicating that a fully reversible one-electron transfer reaction was not achieved. However, a reversible electrode process was achieved for MP-11 in the presence of 25 μM Mg^{2+} (ref. 26 and Table S1–S4 in the electronic supplemental material†). This fact was expected as, at neutral pH, both microperoxidases ($\text{pI} = 4.7$) and the glassy carbon surface are negatively charged. Thus, it was postulated that Mg^{2+} forms a transient bridge between the negatively charged peptide and the electrode surface. The fully reversible electrode process obtained for MP-9 and MP-11 associated to CTAB micelles, in the absence of Mg^{2+} , suggests that the cationic surfactant could also

establish a transient bridge with the electrode surface. The diffusion coefficients of MP-9 and MP-11 associated to CTAB micelles were almost identical to that reported for CTAB micelles ($5.5 \times 10^{-6} \text{ cm}^2 \text{ s}^{-1}$, ref. 27). The diffusion coefficient values obtained in the presence of CTAB were lower than that obtained in water ($1.5 \times 10^{-5} \text{ cm}^2 \text{ s}^{-1}$) indicating that the peptides were associated to the micelles and diffused to the electrode more slowly than in water.

Interestingly, as previously reported and according to UV-visible spectral changes observed when microperoxidases were associated to CTAB micelles,^{21,22} the increase of $\sim 100 \text{ mV}$ in the microperoxidases $E_{1/2}$ was compatible with the lower degree of heme exposure²⁸ and indicates that inside the CTAB micelles, microperoxidases are better oxidant species than exposed to the aqueous medium. Accordingly, the decrease in the diffusion coefficient in the presence of CTAB could only be explained by the presence of the redox entity inside a micellar aggregate.

The MP-9/CTAB and its oxoferryl form can use an aldehyde as reducing agent

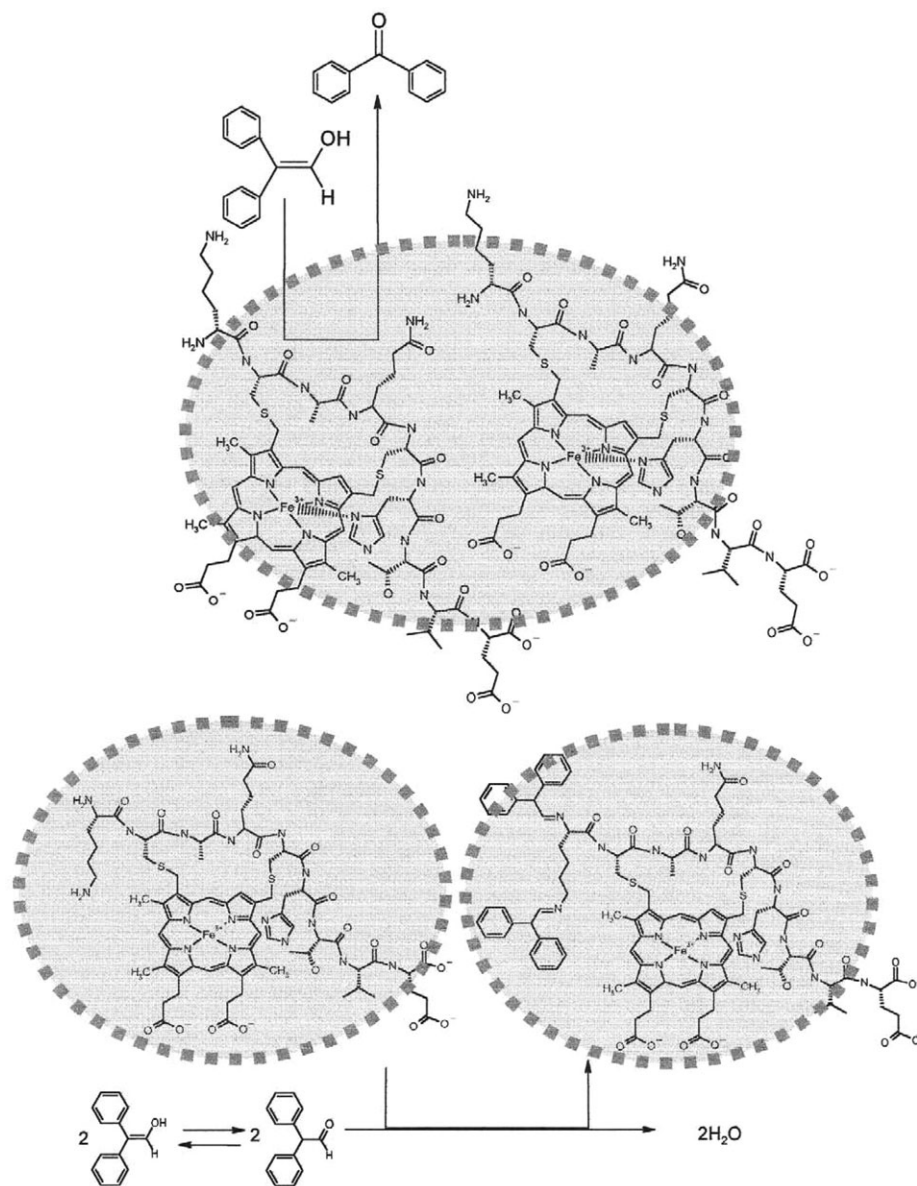
The significant increase in the rate of the conversion of MP-9 Compound II to the native form observed when DPAA was added to the MP-9 oxoferryl species shows that, similarly to peroxidases as HRP,²⁹ MP-9 Compound II can use diphenylacetaldehyde as reducing agent. At the end of the catalytic cycle, when the peroxide was depleted, Fe(III)MP-9/CTAB was able to oxidize DPAA, being converted to the ferrous form, *i.e.*, Fe(II)MP-9 (Fig. 2C and D). HRP was unable to react with DPAA in the absence of peroxides²⁹ but ferric cytochrome *c* could be reduced by DPAA in a pH-dependent manner.³⁰ In the case of cytochrome *c* it was verified that two ionizable groups of the protein with $\text{p}K_{\text{a}} = 8.9$ and $\text{p}K_{\text{a}} = 11.4$, probably Tyr67 and Tyr72, are related to the electron transfer from DPAA to heme iron. Probably, for cytochrome *c* reduction, the stacking of DPAA phenyl rings with tyrosine phenol groups (one ionized and the other protonated) is crucial to electron transfer from DPAA to heme iron. While protonated, cytochrome *c* tyrosine residues stabilize the reduced form of DPAA. On ionization of one cytochrome *c* tyrosine residue, the DPAA enol form increases its electron-donating capability, favoring electron transfer to cytochrome *c* heme iron. Therefore, for cytochrome *c*, the DPAA stacking and the ionization of tyrosine residues are the limiting step in the electron transfer process and not the potential of the aldehyde and the heme iron. In the case of HRP, the inefficiency of DPAA to reduce the enzyme should be expected as the one electron reduction of the heme iron, in non deaerated medium, should lead to the formation of HRP Compound III (ferrous/dioxy/ferric-superoxide complex), an unstable HRP intermediate that rapidly decays to the ferric form.³¹ The lipoenzyme MP-9/CTAB is stable in the reduced form and the reaction is favored probably because the hydrophobic core of the micelle accumulates DPAA, a molecule with low polarity degree. In this regard, the UV-visible spectrum of Fe(II)MP-9/CTAB suggests that the reduced heme iron is coordinated with molecular oxygen as the Q bands are well-defined (Fig. 2C, dashed line) similarly to oxyhemoglobin.^{32,33} Since DPAA can

reduce Fe(III)MP-9 it was expected that the high valence forms of the lipoenzyme could also oxidize this aldehyde increasing the rate of the Compound II to Fe(III)MP-9 conversion.

During the reaction of MP-9/CTAB with DPAA, the yield of the product, benzophenone, was dependent of the micelle/MP-9 molar ratio.

The proposed reaction mechanism (Scheme 3) was corroborated by the identification of benzophenone as the final reaction product (Figs. 4B, 5 and 6). Interestingly, a significant difference in the benzophenone yield could be observed according to the micelle/MP-9 molar ratio (Fig. 4A and B). This difference could be assigned to the accessibility of the amino group to the aldehyde. The analysis of Fig. 4C suggests that the decrease of the micelle/MP ratio favors the association of hemepeptide pairs into the micelle. Only the assumption that at least a couple of MP molecules was occupying one CTAB micelle could explain the MP-9 UV-visible spectra obtained in the CTAB micelle/MP-9 ratio = 0.50 and 0.25. In this regard, the UV-visible spectrum of MP-9 obtained with CTAB micelle/MP-9 ratio = 5.0 seems to be a composite of the spectrum of monomeric MP-9 inside the micelles and dimeric or polymeric MP-9 also inside the micelles. The decrease of the CTAB micelle/MP-9 ratio led to a change of the equilibrium favoring the latter aggregates. In a dimeric association with CTAB micelles, Lys13 amino groups could be forced to locate out of the micelle where the concentration of DPAA was significantly lower due to the partition of the aldehyde, preferentially inside the micelle core. In the monomeric form the Lys13 amino groups could be found inside the micelle core and thus be prone to react with DPAA, leading to the formation of Schiff base adducts. In the monomeric form, the peptide chain of MP-9, being preferentially inside the micelle, could be also prone to being attacked by the intermediate free radicals formed in the course of the reaction. The trapping of the intermediate radicals would decrease the yield of benzophenone without the impairment of the heme iron reduction, a process that precedes the formation of these radicals (Fig. 4A and B). The proposed model was corroborated by the comparison of the MP-9 heme iron EPR spectra obtained with the micelle/MP-9 molar ratio 5.0 and 0.5 (Fig. 4D). In both conditions, MP-9 was predominantly in the high spin form that is in accordance with the proposal that Lys13 α - and ϵ -amino groups could be out of the micelle and not in the micelle core where the reaction intermediate free radicals are generated. The EPR spectra (Fig. 4D), similarly to what was suggested by the UV-visible spectra (Fig. 4C), indicated that different high spin species are favored in different micelle/MP-9 molar ratios. The MP-9/CTAB EPR spectrum obtained at micelle/MP-9 molar ratio = 5.0 reveals higher distortion degree of the axial symmetry of the heme iron as compared with the EPR spectrum obtained at micelle/MP-9 molar ratio = 0.5 since the increase of the micelle/MP-9 molar ratio changed the g shift from 0.070 to 0.259. Scheme 4 illustrates the putative structures of MP-9/CTAB aggregates obtained in low and high micelle/hemepeptide ratios.

The existence of dimeric MP-9 associated to CTAB micelles in low CTAB micelles/MP ratios was reinforced by the heme



Scheme 4 Proposed model for the reaction path of DPAA with MP-9 in CTAB micelles according to the CTAB/MP-9 ratio.

iron EPR spectrum obtained in this condition.²² In the presence of CTAB (micelle/MP ratio = 6.0), only the high spin form of MP-9 was found but with different EPR parameters compared to the high spin state observed in aqueous medium. In CTAB micelles, the prosthetic group exhibits a subtle rhombic distortion, probably due to interactions between the porphyrin rings paired inside the micelle. The characterization of CTAB micelles associated to a pair of microperoxidases concerning the structure and physico-chemical behavior of the aggregate was not the scope of the present work and is under investigation in our laboratories.

Conclusion

Important findings can be outlined from this work:

- The determination of the redox potential of the previously described lipoenzyme MP/CTAB.

- The exclusive ability of both Compound II and Fe(III)MP-9/CTAB to oxidize DPAA contrary to HRP that can only do it in the high valence states and cytochrome *c*, only the alkaline pH values.

- The high yield of benzophenone production obtained with the catalyst MP-9/CTAB, which was not observed for the previously studied enzymes: HRP and cytochrome *c*. In this regard it is important to extend the future investigation to other substrates concerning application of this catalyst in nanotechnology.

- The possibility to modulate the reaction mechanism of aldehydes' oxidation according to the MP/CTAB ratio, also important for future application of this catalyst.

Acknowledgements

We are grateful for the Brazilian research funding agencies FAPESP (Fundação de Amparo à Pesquisa do Estado de São

Paulo), FAEP-UMC (Fundação de Amparo ao Ensino e Pesquisa da Universidade de Mogi das Cruzes), CAPES (Coordenadoria de Aperfeiçoamento de Pessoal de Ensino Superior) and CNPq (Conselho Nacional de Pesquisa) as well as the John Simon Guggenheim Memorial Foundation (P.D.M. Fellowship) for their financial support. T.P. is CAPES fellow and R.O.M. is FAPESP fellow.

References

- 1 P. G. Furtmüller, M. Zederbauer, W. Jantschko, J. Helm, M. Bogner, C. Jakopitsch and C. Obinger, *Arch. Biochem. Biophys.*, 2006, **445**, 199–213.
- 2 C. Colas, J. M. Kuo and P. R. Ortiz de Montellano, *J. Biol. Chem.*, 2002, **277**, 7191–7200.
- 3 L. Huang, G. Wojciechowski and P. R. Ortiz de Montellano, *J. Am. Chem. Soc.*, 2005, **5127**, 5345–5353.
- 4 B. Bhaskar and T. L. Poulos, *J. Biol. Inorg. Chem.*, 2005, **10**, 425–430.
- 5 R. Perera, M. Sono, J. A. Sigman, T. D. Pfister, Y. Lu and J. H. Dawson, *Proc. Acad. Natl. Sci. U. S. A.*, 2003, **100**, 3641–3646.
- 6 A. D. Carraway, S. L. Povlock, M. L. Houston, D. S. Johnston and J. Peterson, *J. Inorg. Biochem.*, 1995, **60**, 267–276.
- 7 C. Veeger, *J. Inorg. Biochem.*, 2002, **91**, 35–45.
- 8 J. Peterson, M. M. M. Saleem, J. Silver and M. T. Wilson, *J. Inorg. Biochem.*, 1983, **19**, 165–178.
- 9 V. S. Sharma, M. R. Schmidt and H. M. Ranney, *J. Biol. Chem.*, 1976, **251**, 4267–4272.
- 10 K. Kimura, J. Peterson, M. T. Wilson, D. J. Cookson and R. J. Williams, *J. Inorg. Biochem.*, 1981, **15**, 11–25.
- 11 T. Tatsuma and T. Watanabe, *Anal. Chem.*, 1992, **64**, 143–147.
- 12 H. B. Dunford and J. S. Stillman, *Coord. Chem. Rev.*, 1975, **19**, 187–251.
- 13 H. K. Baek and H. E. Van Wart, *Biochemistry*, 1989, **29**, 5714–5719.
- 14 J. S. Wang, K. B. Haesun and H. E. Van Wart, *Biochem. Biophys. Res. Commun.*, 1991, **179**, 1320–1324.
- 15 G. Berglund, G. H. Carlsson, A. T. Smith, A. Szöke Henriksen and J. Hajdu, *Nature*, 2002, **417**, 463–468.
- 16 M. Mukai, S. Nagano, M. Tanaka, K. Ishimori, I. Morishima, T. Ogura, Y. Watanabe and T. Kitgawa, *J. Am. Chem. Soc.*, 1997, **119**, 1758–1766.
- 17 P. R. Ortiz de Montellano, *Annu. Rev. Pharmacol. Toxicol.*, 1992, **32**, 89–107.
- 18 M. I. Savenkova, J. M. Kuo and P. R. Ortiz de Montellano, *Biochemistry*, 1998, **37**, 10828–10836.
- 19 A. T. Smith and N. Veitch, *Curr. Opin. Chem. Biol.*, 1998, **2**, 269–278.
- 20 J. L. Primus, S. Grunenwald, P. L. Hagedoorn, A.-M. Albrecht-Gary, D. Mandon and C. Veeger, *J. Am. Chem. Soc.*, 2002, **124**, 1214–1221.
- 21 T. Prieto, O. R. Nascimento, I. L. S. Tersariol, A. Faljoni-Alario and I. L. Nantes, *J. Phys. Chem. B*, 2004, **108**, 11124–11132.
- 22 T. Prieto, O. R. Nascimento and I. L. Nantes, *Prog. Colloid Polym. Sci.*, 2004, **128**, 193–198.
- 23 J. Aron, D. A. Baldwin, H. M. Marques, J. M. Pratt and P. A. Adams, *J. Inorg. Biochem.*, 1986, **27**, 227–243.
- 24 E. Canpolat and M. Kaya, *Turk. J. Chem.*, 2005, **29**, 409–415.
- 25 J. Fabian, M. Legrand and P. Poirier, *Bull. Soc. Chim. Fr.*, 1956, **23**, 1499–1509.
- 26 M. J. Eddowes, H. A. O. Hill and K. Uosaki, *Bioelectrochem. Bioenerg.*, 1980, **7**, 527–537.
- 27 *Handbook of Chemistry and Physics*, ed. David R. Lide, CRC Press, Boca Raton, FL, USA, 82nd edn, 2001–2002, pp. 5–96.
- 28 E. Stellwagen, *Nature*, 1978, **275**, 73–74.
- 29 I. L. Nantes, G. Cilento and E. J. H. Bechara, *Photochem. Photobiol.*, 1996, **62**, 522–527.
- 30 T. A. Rinaldi, I. L. S. Tersariol, F. Dyszy, F. M. Prado, O. R. Nascimento, P. Di Mascio and I. L. Nantes, *Free Radical Biol. Med.*, 2004, **36**, 802–810.
- 31 C. Jakopitsch, A. Wanasinghe, W. Jantschko, Furtmüller and C. Obinger, *J. Biol. Chem.*, 2005, **280**, 9037–9042.
- 32 I. L. Nantes, M. R. Zucchi, O. R. Nascimento and A. Faljoni-Alario, *J. Biol. Chem.*, 2001, **276**, 153–158.
- 33 W. A. Eaton and J. Hofrichter, *Methods Enzymol.*, 1981, **76**, 175–261.